Volume 1 | Number 1 | Jan 2013 | Pages 1–100

Dalton Transactions

An international journal of inorganic chemistry
www.rsc.org/dalton

ROYAL SOCIETY OF CHEMISTRY

ROYAL SOCIETY OF CHEMISTRY

www.rsc.org/dalton

In Situ Microcalorimetry Study of $ZnFe_2O_4$ Nanoparticle Formation under Solvothermal Conditions

Jun Liu[a], Zhaodong Nan[a, *], Shengli Gao[b, *]

[a] College of Chemistry and Chemical Engineering, Yang Zhou University, Yangzhou, 225002, China

[b] Key Laboratory of Synthetic and Natural Functional Molecule Chemistry of Ministry of Education, College of Chemistry & Materials Science, Northwest university, Xi'an 710069, China

*Corresponding author. E-mail addresses: zdnan@yzu.edu.cn (Z. Nan), gaoshli@nwu.edu.cn (S. Gao)

1

ABSTRACT: A solvothermal method has been widely used to synthesize different kinds of materials. However, only little is known about how precursor solutions react to form solid precipitates by using this method. At present, in situ microcalorimetry is first used to investigate the formation mechanism under solvothermal conditions, where $ZnFe_2O_4$ synthesized by a solvothermal method was selected as a model sample. Some novel results are obtained, such as with the experimental temperature increase, (1) the homogeneous solution transforms to a gel contained amorphous $Fe_2(C_2H_4O_2)_3$ and $ZnC_2H_4O_2$, and $NaNO_3$ crystals; (2) the gel dissolves; (3) α-(Fe, Zn)OOH and α-Fe_2O_3 are synthesized; (4) the α-(Fe, Zn)OOH transforms to α-Fe_2O_3; (5) Fe^{2+} is formed at about 159 ^{o}C, which acted as a catalyst for the formation of Fe_3O_4; (6) the Fe_3O_4 crystals are synthesized at about 200 ^{o}C; (7) the Fe_3O_4 is transformed to the $ZnFe_2O_4$ with the help of the NO_3^-, and the reaction was end at 200 ^{o}C for about 20 h. This study shows a facile in situ method for investigation on the reaction progresses for solvothermal methods.

1. Introduction

As one of experimental methods, a solvothermal process is famous for its unique control facilities regarding the particle size of the precipitates.[1, 2] At present, only little is known about how precursor solutions react to form solid precipitates and eventually transform into nanocrystals under solvothermal conditions.[3] These processes occurring during the early stages of the solid nanocrystals formation are not well understood, so the rational synthesis of new materials are prevented. To study the structure-forming process is an enormous challenge for both analytical and theoretical methods because very small particles or aggregates with different chemical compositions and sizes must be probed. Furthermore, these precursors are present in a complex and dynamic equilibrium under the experimental conditions. In situ methods are available for the study of the forming progresses of the solid nanocrystals and can help in the determination of metastable polymorphs, of transient intermediates, and/or precursors displaying new or improved properties. It has been demonstrated the necessity and potentials to monitor the solid nanocrystals formation by applications of in situ methods.[4] These methods are powerful tools for studying solvothermal synthesis mechanisms because they can monitor the synthesis by collecting time-resolved patterns containing direct reaction information, such as phase evolution and the fate of the transient reaction intermediates. To obtain the reaction intermediates is critical in determining reaction mechanisms, but the intermediates can be missed by ex situ techniques.[5] Applications of in situ techniques are gaining tremendous attention, however, there are very few examples in which these methods have been applied to study reaction mechanisms of nanoparticle formation under

elevated temperature and pressure conditions, especially during the increasing temperature progress.[6] The application of in situ technology has been reported, such as in situ powder X-ray diffraction (PXRD) and in situ small angle X-ray scattering (SAXS),[5] and EDXRD (energy dispersive X-ray diffraction) and XANES/EXAFS (X-ray absorption near edge structure/extended X-ray absorption fine structure) techniques,[7] which often require sophisticated equipments, and amorphous solids and small particles (typically below 5 nm) cannot be detected by Bragg diffraction. In situ monitoring technology is still under development in the field of the investigation on nanocrystals formation under solvothermal conditions.

Calorimetry is spectroscopy without selection rules.[8] Therefore, as a nondestructive, fast, and inexpensive technique, this technology can be used to probe the formation of nanocrystals under a solvothermal method in situ. Easy to set up and interpret, this approach can be conveniently applied for online analyses during the materials formation. This method has been applied to study the formation mechanisms of different materials, such as $Zn(Met)(AcO)_2 \cdot H_2O$,[9] silica TPA-MFI zeolite (TPA = tetrapropylammonium, MFI) framework structure code of ZSM-5,[10] CdS nanocrystals,[11] and MCM-41 mesoporous silica.[12] However, the experimental temperature was always kept a constant during these experimental processes. There is only one example in which a hydrothermal processing was studied by using in situ calorimetry for ZnO formation as far as we know.[13]

Colloidal nanoparticle clusters (NCs) formed by clustering nanoparticles into secondary structures allow the combination of properties of individual nanoparticles

and takes advantage of the interactions between neighboring nanoparticles which can result in new properties not present in the original constituents.[14] For example, forming magnetic ferrite NCs has proved to be an effective way to retain superparamagnetic behavior with high magnetization.[15-17] A polyol method was developed for the preparation of these kinds of magnetic NCs, such as Fe_3O_4 and $ZnFe_2O_4$ et al., through the hydrolysis and reduction in an ethylene glycol solution at high temperatures (about 200 ^{o}C).[15] The mechanism for this solvothermal method was reported, in which Fe^{3+} is reduced by ethylene glycol to Fe^{2+} firstly, Fe_3O_4 is synthesized.[15a] However, the temperatures corresponding to these reactions and the changing processes from room temperature to 200 ^{o}C have not been studied, which induced the reaction mechanism cannot be investigated in details.

Hence this work was undertaken to gain an understanding of the solvothermal crystallization mechanism for the formation of the magnetic $ZnFe_2O_4$ NCs from room temperature to 200 ^{o}C by a microcalorimetry technique. The synthesis mechanism has been elucidated based on the information obtained by in situ microcalorimetry, in which the changes of the reaction system are as the following with the experimental temperature increase from room temperature to 200 ^{o}C, (1) a homogeneous solution contained $Fe(NO_3)_3$, $Zn(NO_3)_2$, and NaAc; (2) ethylene glycol sol and gel contained $Fe_2(C_2H_4O_2)_3$, $ZnC_2H_4O_2$, and $NaNO_3$; (3) a homogeneous solution; (4) α-(Fe, Zn)OOH; (5) α-Fe_2O_3; (6) Fe_3O_4; and (7) $ZnFe_2O_4$. Based on the present results, it can be explained that Fe^{3+} could not be reduced by ethylene glycol without NaAc, and the reaction temperature is necessary to keep at 200 ^{o}C. Our aim of this paper hopes to

introduce this kind of in situ technique to study the mechanism for materials formation under the solvothermal conditions.

2 Experimental

2.1 Materials

All chemicals, such as ferric nitrate nonahydrate ($Fe(NO_3)_3 \cdot 9H_2O$), zinc nitrate hexahydrate ($Zn(NO_3)_2 \cdot 6H_2O$), sodium acetate (CH_3COONa), ethylene glycol ($C_2H_6O_2$), benzene (C_6H_6), sodium ethoxide (C_2H_5ONa), 2,4-Dinitrophenylhydrazine ($C_6H_6N_4O_4$), anhydrous ethanol (C_2H_6O), and acetone (C_3H_6O) were analytical grade regents from the Sinopharm Chemical Reagent Company and used as starting materials without further purification.

2.2 Synthesis

The sample preparation is at synchronization with the microcalorimetry listed in the underside. In a typical experiment, 3.0 mmol $Zn(NO_3)_2 \cdot 6H_2O$ and 6.0 mmol $Fe(NO_3)_3 \cdot 9H_2O$ were dissolved in 25 mL of anhydrous ethylene glycol. Then, 9.0 mmol CH_3COONa (NaAc) was added into the solution. The whole mixture was stirred vigorously for 5 min to give a homogeneous solution. Subsequently, the solution was transferred into a 50 mL conical flask with a ground cover, and put into a electrothermal blowing dry box, and the temperature increased at 5 $^oC/h$. The conical flask was taken out based on the microcalorimetric result. The precipitate was separated by centrifugal separation, and dried under vacuum at 80 ^oC for 24 h.

2.3 Microcalorimetry

The calorimetric experiment was performed using a C-80 microcalorimeter with

sensitivity of 0.10 mW produced by SETARAM (France). Temperature accuracy, temperature precision, and calorimetric precision are +/- 0.1 ^{o}C, +/- 0.05 ^{o}C, and +/- 0.1 %, respectively. The working temperature range of the microcalorimeter is from ambient temperature to 300 ^{o}C. At the present experiment, the experimental temperature was changed from room temperature to 200 ^{o}C with 5 ^{o}C/h and kept at 200 ^{o}C for 24 h, and a couple of high press cells (8 mL) were used. 5 mL of homogeneous solution contained 0.12 M $Zn(NO_3)_2 \cdot 6H_2O$, 0.24 M $Fe(NO_3)_3 \cdot 9H_2O$, and 0.36 M NaAc (as prepared above) was put into the sample cell, and 5 mL of ethylene glycol was put in the reference cell .

2.4 Characterization

X-ray powder diffraction (XRD) measurements were performed on a Bruker D8 Advance X-ray Diffractometer with Cu Kɑ radiation (λ=1.5418Å). The 2θ range used in the measurement was from 10 to 80º. Standard Scanning electron microscopy (SEM) measurements were performed on a HITACHI S-4800Ⅱ (Hitachi LTD. Japan) at an acceleration voltage of 200 kV. The metal ion (Fe and Zn) concentration was measured by inductively coupled plasma atomic emission spectroscopy (ICP-OES) on an Optima7300 DV (Perkin Elmer), and the metal ion (Na) concentration was measured by atomic absorption spectrophotometer (AAS) on a PE-2100 (Perkin Elmer). The chemical compositions of the MNCs were determined by the dissolution of 0.2200 g of the sample in 10 mL of 35 wt% HCl solution, followed by the diluting it to 1000 ml. X-ray photoelectron spectroscopy (XPS) measurements were performed using a Thermo VG Thermo Scientific Escalab 250 fitted with a monochromotized

X-ray Al Kα (1486.8 eV) source. A 150 W X-ray spot of 500 μm in diameter was used

for survey scans. Charge neutralization was accomplished by a low-energy electron

flooding. All spectra were referenced to the C 1s peak at 284.8 eV. Infrared spectrum

(FT-IR) measurements were performed on a Nicolet Aexus 470, with scanning

from4000 to 400 cm^{-1} by using KBr pellets under ambient temperature. Ultraviolet

spectrophotometry (UV) were performed on a UV2500, with scanning from400 to

800 nm. Thermogravimetric analysis (TGA) was performed under argon flow from 50

to 800 ^{o}C using a NETZSCH ST9449 Thermogravimetric Analyzer. UV-Vis spectra

were taken with a UV-2500, produced in Shimadzu Co. based on a reference.[18] In

details, 0.2 mL of the solutions obtained at different temperatures based on the

calorimetric curve was added to 1.0 mL of DNPH (2,4-Dinitrophenylhydrazine)

solution (0.0494 g of DNPH in 50.0 mL of 35 wt% hydrochloric acid and diluted to

100.0 mL with distilled water) and 20.0 mL of water, The hydrazone is then extracted

by 20.0 mL of benzene and the solution was made alkaline with sodium ethoxide

solution (10.0 mL of 2.9000 g of sodium ethoxide in 100.0 mL of ethanol). The

resulting emulsion is diluted with 20.0 mL of ethanol and centrifuged to increase its

optical transparency, and then an absorbance spectrum was taken.

3 Results and discussion

A typical microcalorimetric curve for $ZnFe_2O_4$ NCs growth is shown in Fig. 1, in

which no change can be found from room temperature to about 80 ^{o}C, about seven

peaks are determined with further increasing temperature and the corresponding

temperatures are determined as listed in Table 1. Eight samples are selected corresponding to crests and troughs of these peaks named as *B*, *C*, *D*, *E*, *F*, *G*, *H*, and *I*, as shown in Fig. 1. In order to study the early stage, *A* is selected before the first peak appeared. The change processes at 200 °C for this system was studied in our previous report.[17] Thus, a sample was only selected as *I* at the starting 200 °C. The heat flow returned to zero when the temperature kept 200 °C for about 20 h. The details for the analysis of the curve by thermodynamic software (AKTS, Switzerland) are shown in the supporting information (Fig. S1).

Fig. 2 presents the photographs of the samples obtained under different temperatures based on the typical microcalorimetric curve. It can be found from these photographs that the original solution (*OS*), *A*, and *F* were black solutions, the samples *B*, *C*, and *E* were mixtures contained solutions and gels, *D* was a gel, and the samples *G*, *H*, and *I* included precipitates and solutions as listed in Table 1. When the experimental temperature decreased to about 20 °C, the samples *B*, *C*, *D*, and *E* changed to homogeneous solutions after a week, respectively, which demonstrates that the gel formation is a reversible process. Thus, the changing processes for the present system are depicted as solution-sol –gel – solution - solid sample.

XRD patterns of the samples obtained at different reaction temperatures are showed in Fig. 3, in which all diffraction peaks of the samples *B*, *C*, *D* and *E* were indexed to $NaNO_3$ (ICDD no. 36-1474), diffraction peaks of the samples *G* and *H* were indexed to α-(Fe, Zn)OO[19] and α-Fe_2O_3 (ICDD no. 65-0390), and diffraction peaks of the sample *I* were indexed to α-Fe_2O_3 (ICDD no. 65-0390), and Fe_3O_4

(ICDD no. 28-0491) and/or $ZnFe_2O_4$ (ICDD no. 22-1012). The peaks corresponding

to $NaNO_3$ were enhanced from the samples B, C to D, and weakened from D to E. No

peak corresponding to $NaNO_3$ can be found for the samples G, H, and I.

It was reported that ethylene glycol deprotonated and coordinated with Ce^{3+} and

Fe^{3+} to form cerium and iron alkoxides.[20, 21] At the present conditions, we assumed

that Fe^{3+} and Zn^{2+} formed alkoxides. Analysis results of ICP-OES and AAS for the

metal ions (Fe^{3+}, Zn^{2+}, and Na^+) are listed in Table 2, in which demonstrates that the

compositions of the as-prepared samples are consistent with the formation of (Fe^{3+},

Zn^{2+}) alkoxides and $NaNO_3$, especially for the samples C and D. The Fe^{3+} and Zn^{2+}

alkoxides synthesized at the present are amorphous based on the XRD results, which

are different with references.[20, 21] In the most cases the as-synthesized precipitates are

amorphous and subsequent heat treatment is necessary to induce crystallization for

sol-gel processes.[22]

Thermal decomposition behaviors of the samples B, C, D and E under argon

atmosphere were monitored by TG and DTG as shown in Fig. 4, in which three

noticeable weight loss stages can be observed. The first was occurred from 77 to 177

^{o}C, which was ascribed to the evaporation of the H_2O adsorbed on the sample surface.

The second was occurred from 240 to 320 ^{o}C, which was ascribed to the

decomposition of the alkoxides ($Fe_2(C_2H_4O_2)_3$ and $ZnC_2H_4O_2$).[23] The third was

occurred from 320 to 380 ^{o}C, which was ascribed to the decomposition of the

$NaNO_3$.[24] These results demonstrate the formations of $Fe_2(C_2H_4O_2)_3$, $ZnC_2H_4O_2$ and

$NaNO_3$.

Fourier transform infrared (FT-IR) analysis was performed to identify the structure and the functional groups of the samples *B, C, D* and *E* as shown in Fig. 5. The bands around 1620 and 3440 cm^{-1} were attributed to the O-H bending vibration and the O-H stretching vibration.[25] The bands around 440, 527, 830, 1080 cm^{-1} were attributed to the Zn-O vibration, Fe-O bond vibration, C-C bond vibration, C-O bond vibration, respectively.[26-28] The two bands around 2840 and 2880 cm^{-1} were attributed to the CH$_2$- symmetrical stretching vibration and asymmetrical stretching vibration, respectively. These results indicated the presence of Fe$_2$(C$_2$H$_4$O$_2$)$_3$ and ZnC$_2$H$_4$O$_2$ in the samples *B, C, D* and *E*.[29] The band around 1380 cm^{-1} was the asymmetric stretching vibration of NO$_3^-$,[25] which indicated the presence of NaNO$_3$.

Fig. 6 shows XPS survey spectra of the samples *D, E, G, H*, and *I*. Peak values at 1072, 1047.9, 1022.4, 729.1, 713.1, 531.4, 407, and 284.8 eV can be indexed to binding energies of Na 1s, Zn 2p$_{1/2}$, Zn 2p$_{3/2}$, Fe 2p$_{1/2}$, Fe 2p$_{3/2}$, O 1s, N 1s, and C 1s, respectively, which confirmed the existence of Na, Zn, Fe, O, N and C elements in the samples.

The Fe2p XPS spectra of these samples are shown in the supporting information as Fig. S2. The spectra were fitted with Gaussian function,[30] and the Fe 2p$_{3/2}$ broad could be divided into 3 sub-peaks. For samples *D* and *E*, the energy peaks at 710.4, 711.0 and 713.1 eV were corresponding to the Fe^{3+} with different chemical environment.[31-33] For the sample *G*, the energy peaks at 709.5 eV was corresponding to the Fe^{2+},[34] and both of the two energy peaks at 710.7 and 711.6 eV were corresponding to the Fe^{3+} in FeOOH.[31, 35] For the sample *H*, the energy peaks at 709.5,

710.5 and 711.6 eV were corresponding to the Fe^{2+},[34] the Fe^{3+} in α-Fe_2O_3 and the Fe^{3+} in FeOOH.[35, 36] For the sample *I*, the energy peaks at 709.2, 710.5 and 711.1 eV were corresponding to the Fe^{2+} in Fe_3O_4,[37] the Fe^{3+} in α-Fe_2O and the Fe^{3+} in Fe_3O_4.[36, 38] Obviously, the Fe2p XPS spectra of the samples *D* and *E* were similar, it indicated that the chemical environment for Fe element have not been changed as the temperature increased from 107 to 118 ^{o}C. Remarkable, the Fe^{2+} was not appeared until the temperature reached 159 ^{o}C, which was agreement with the UV analysis result as the following that the redox reaction between Fe^{3+} and EG was occurred when the temperature increased at 159 ^{o}C. And as the temperature increased from 159 to 200 ^{o}C, the characteristic peaks for the Fe^{3+} in FeOOH, α-Fe_2O_3, and Fe_3O_4 appeared orderly, it was conform with XRD analysis that the transformation processes of the precursor were as α-(Fe, Zn)OOH to α-Fe_2O_3 to Fe_3O_4.

The O1s XPS spectra of these samples *D*, *E*, *G*, *H* and *I* are shown in the supporting information as Fig. S3. For the sample *D*, the sub-peaks at 529.4 and 531.1 eV were corresponding to the lattice oxygen and the O in OH⁻, respectively.[35, 39] The sub-peak at 533.0 eV was similar to the O in C-O (532.8 eV).[40] Similar results were obtained for the sample *E* with three sub-peaks at 529.5, 531.1 and 532.6 eV. For the samples *G* and *H*, three sub-peaks at 528.9, 530.3 and 531.3 eV were corresponding to the O in oxyhydroxide,[36, 41] FeOOH and OH⁻, respectively.[33, 35] For the sample *I*, three sub-peaks at 528.8, 530.3 and 530.9 eV were corresponding to the O in oxyhydroxide,[35] Fe_3O_4 and metallic oxide, respectively.[37, 42] Remarkably, the energy peak at 530.3 eV could be corresponding to the O in FeOOH and Fe_3O_4.[33, 37]

According to the XRD analysis, for the samples *G* and *H*, the peak at 530.3 eV was corresponding to the O in FeOOH, and for the sample *I*, this peak was corresponding to the O in Fe_3O_4.

The N1s XPS spectra of these samples are shown in the supporting information as Fig. S4. For the sample *D*, there was only one energy peak at 407.4 eV, which was similar to the N in $NaNO_3$ (407.3 eV).[38] The spectra of sample *E* had large full widths at half maximum (FWHM), which was divided into 2 sub-peaks. The energy peak at 407.2 eV was similar to the N in $NaNO_3$, and the energy peak at 406.0 eV was corresponding to the N in nitro-compound.[38] The difference of the N1s XPS spectra between the samples *D* and *E* would be caused by the NO_3^- chemical reaction with the temperature increased from 107 to 134 ^{o}C. The detailed mechanism needs a further study. Furthermore, there was not any peak corresponding to N for the samples *E*, *H* and *I*.
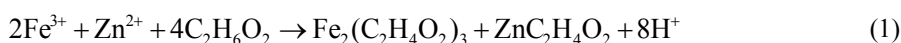
The Zn2p XPS spectra of these samples are shown in the supporting information as Fig. S5. All samples have only two energy peaks at 1021.0 and 1044.0 eV, which were corresponding to $Zn2p_{3/2}$ and $Zn2p_{1/2}$. Besides, the spin orbit splitting of 23 eV indicates that the ion valence state is Zn^{2+}.[39]

UV analysis can be used to study the EG oxidation, in which 2, 4-dinitrophenylhydrazine was used as an indicator.[18] Fig. 7 shows UV spectra of the solutions obtained at different temperatures, in which a peak at 570 nm corresponding to glyoxal bis-2,4-dinitrophenylhydrazone was firstly discovered at 159 ^{o}C, and enhanced with the temperature increasing to 200 ^{o}C. And this peak strengthened

rapidly when the temperature increased from 187 to 200 ^{o}C. The Fe^{2+} was firstly determined for the sample G (159 ^{o}C) based on XPS. These results indicated that a redox reaction between EG and Fe^{3+} was occurred initially at 159 ^{o}C and the products were glyoxal and Fe^{2+}, respectively. However, no Fe_3O_4 was determined by XRD at this temperature. The reasons may be that the Fe^{2+} cannot reach the critical concentration for Fe_3O_4 crystal formation, and the Fe_3O_4 crystals were synthesized with the experimental temperature increasing to about 200 ^{o}C as shown in Fig. 3. The peak at 570 nm in Fig. 7 demonstrates that the concentration of the glyoxal was significantly higher when the experimental temperature increased from 187 to 200 ^{o}C. Xia et al. reported that glycolaldehyde was synthesized from EG at 150 ^{o}C.[18] The oxidation of EG to glyoxal requires both heat and nitric acid.[43] At the present conditions, nitric acid was formed at the early stage in the reaction system, and the glyoxal was synthesized.

Typical SEM images of the samples are shown in Fig. 8, in which different morphologies of particles are found. For the samples B, C, D, and E, a kind of regular hexahedron is shown especially in C and D, which may be corresponding to $NaNO_3$ crystals based on XRD results. Compared with the samples B, C, D, and E, the morphology of the samples G, H, and I changed significantly.

Based on the results listed above, a mechanism for the $ZnFe_2O_4$ formation is proposed as the following. When the experimental temperature increased at about 80 ^{o}C, the alkoxides ($Fe_2(C_2H_4O_2)_3$ and $ZnC_2H_4O_2$), and $NaNO_3$ were synthesized.

$$2Fe^{3+} + Zn^{2+} + 4C_2H_6O_2 \rightarrow Fe_2(C_2H_4O_2)_3 + ZnC_2H_4O_2 + 8H^+ \qquad (1)$$

14

$$Na^+ + NO_3^- \rightarrow NaNO_3 \tag{2}$$

At this process, plentiful H^+ was formed as eq. (1). In order to neutralize the H^+, the following equation was taken place.

$$CH_3COO^- + H^+ \rightarrow CH_3COOH \tag{3}$$

At the same time, the following equation may be occurred in the present system because the NO_3^- concentration is higher than the Na^+.
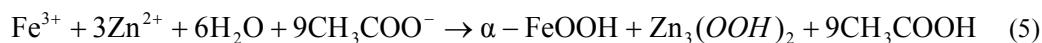
$$NO_3^- + H^+ \rightarrow HNO_3 \tag{4}$$

The metal alkoxide species can also be produced in situ by the alcoholysis of metal halides.[22] At the present conditions, $Fe_2(C_2H_4O_2)_3$ and $ZnC_2H_4O_2$ were formed by the alcoholysis of $Fe(NO_3)_3$ and $Zn(NO_3)_2$ as eq(1).

As references reported, when EG coordinated with $FeCl_3$ and $SnCl_2$ to form alkoxides, HCl was a byproduct, and urea was used to neutralize the HCl and allowed the coordination reaction to be completed.[44, 45] At the present conditions, HNO_3 and CH_3COOH were formed.

Between 90 (the sample *A*) to 99 ^{o}C (the sample *B*), EG sol and gel were found until to 107 ^{o}C (the sample *D*). So the first peak in Fig. 1 was corresponding to eqs (1-4), and the second peak corresponding to the gel formation. When the experimental temperature increased to 107 ^{o}C, the gel began to dissolve, and it became a homogenous solution at 118 ^{o}C (the sample *F*). As reported, metal alkoxides constitute the most widely used class of precursors in sol–gel processes.[46, 47]
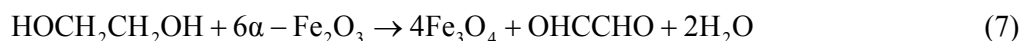
α-(Fe, Zn)OOH and α-Fe$_2$O$_3$ were determined for the sample *G* obtained at 159 ^{o}C.

Thus, the third peak in Fig. 1 was corresponding to the dissolving of the gel, and

α-(Fe, Zn)OOH and α-Fe$_2$O$_3$ formation.

$$Fe^{3+} + 3Zn^{2+} + 6H_2O + 9CH_3COO^- \rightarrow \alpha - FeOOH + Zn_3(OOH)_2 + 9CH_3COOH \quad (5)$$

$$2\alpha \text{-} FeOOH \rightarrow \alpha \text{-} Fe_2O_3 + H_2O \quad (6)$$

Where α-FeOOH and Zn$_3$(OOH) formed a solid solution as expressed as α-(Fe,

Zn)OOH.

At the same time, the following redox reaction was occurred in the experiment,

where the Fe$_3$O$_4$ is not crystal.

$$HOCH_2CH_2OH + 6\alpha - Fe_2O_3 \rightarrow 4Fe_3O_4 + OHCCHO + 2H_2O \quad (7)$$

The fourth peak in Fig. 1 was corresponding to the reaction as (6) and (7) based on the

results obtained from Fig. 3. And no Fe$_3$O$_4$ crystals were determined at 187 ^{o}C for the

sample *H*. In Fig. 3, the peak corresponding to α-Fe$_2$O$_3$ was enhanced, and about no

α-(Fe, Zn)OOH was determined when the experimental temperature increased from

187 to 200 ^{o}C. These results demonstrated that the reactions as (6) and (7) were still

occurred in the reaction system, and the Fe$_3$O$_4$ crystals were formed. Based on the

results listed in Table 2 and Fig. S5, Zn^{2+} was contained in the sample *I*, which

induced that the peaks at about $2\theta \approx 35$ ^{o} may be corresponding to a mixture of Fe$_3$O$_4$

and ZnFe$_2$O$_4$. The following reactions were taken place.

$$Fe_3O_4 + Zn^{2+} \rightarrow ZnFe_2O_4 + Fe^{2+} \quad (8)$$
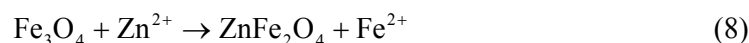
The as-prepared Fe^{2+} was reduced to Fe^{3+} by NO$_3^-$, which induced the reaction (8)

to reach about completely.[17] In the present conditions, Fe^{3+} and Zn^{2+} are present in the

system, and no $Zn_xFe_{3-x}O_4$ was determined until at 200 ^{o}C. Fe^{2+} was synthesized after

159 ^{o}C, and the reaction (7) was enhanced at 200 ^{o}C. Based on these results, we

proposed that Fe_3O_4 was synthesized firstly, which is consistent with our previous

report.[17, 45] The $Zn_xFe_{3-x}O_4$ crystal was less stable than the Fe_3O_4 one.[48] Thus, the Fe^{2+},

as a metastable interproduct, acts as a catalyst to form $ZnFe_2O_4$ crystals.

Stoichiometric $ZnFe_2O_4$ was synthesized at 200 ^{o}C for 24 h,[17] the heat flow returned

to zero when the temperature kept 200 ^{o}C for about 20 h.

4 Conclusions

In summary, a plausible mechanism was proposed for $ZnFe_2O_4$ NCs growth

process based on the in situ microcalorimetry. Combination other determineded

techniques, the reaction mechanism for the present study was as the following. When

the experimental temperature increased, the homogeneous solution transformed to the

gel contained amorphous $Fe_2(C_2H_4O_2)_3$ and $ZnC_2H_4O_2$, and $NaNO_3$ crystals; the gel

dissolved and α-(Fe, Zn)OOH and α-Fe_2O_3 were synthesized; α-(Fe, Zn)OOH

transformed to α-Fe_2O_3; Fe^{2+} was formed at about 159 ^{o}C, which acted as a catalyst

for the formation of Fe_3O_4; the Fe_3O_4 crystals were synthesized at about 200 ^{o}C; and

the Fe_3O_4 was transformed to the $ZnFe_2O_4$ with the help of the NO_3^-. Based on the

formation mechanism, we can modify the properties of the samples through the

addition of additives (not shown here). These results will be further studied. This kind

of in situ technique may be very useful to facilely study the reaction mechanism for

different solvothermal methods.

Acknowledgements

References

1   R. I. Walton, *Chem. Soc. Rev.* **2002**, *31*,230-238.

2   G. Demazeau, *J. Mater. Chem.* **1999**, *9*,15-18.

3   D. Saha, K. M. Ø. Jensen, C. Tyrsted, E. D. Bøjesen, A. H. Mamakhel, A. C. Dippel, M. Christensen, B. B. Iversen, *Angew. Chem*. **2014**, *126*, 1 – 5.

4   N. Pienack, W. Bensch, *Angew. Chem. Int. Ed.* **2011**, *50*, 2014 – 2034.

5   F. Xia, D. Chen, N. V. Y. Scarlett, I. C. Madsen, D. Lau, M. Leoni, J. Ilavsky, H. E. A. Brand, R. A. Caruso, *Chem. Mater.* **2014**, *26*, 4563−4571.

6   (a) K. M. Ø. Jensen, M. Christensen, P. Juhas, C. Tyrsted, E. D. Bøesen, N. Lock, S. J. L. Billinge, B. B. Iversen, *J. Am. Chem.Soc*. **2012**, *134*, 6785 – 6792; (b) C. Tyrsted, K. M. Ø. Jensen, E. D. Bøesen, N. Lock, M. Christensen, S. J. L. Billinge, B. B. Iversen, *Angew. Chem.* **2012**, *124*, 9164 – 9167; (c) C. Tyrsted, K.M.Ø. Jensen, E.D. BØjesen, N. Lock, M. Christensen, S.J.L. Billinge, B.B. Iversen, Angew. Chem. Int. Ed. **2012**, *51*, 9030 – 9033.

7   A. Michailovski, J. D. Grunwaldt, A. Baiker, R. Kiebach, W. Bensch, G. R. Patzke, *Angew. Chem. Int. Ed.* **2005**, *44*, 5643 −5647.

8   A. Navrotsky, *J. Chem. Thermodynamics* **2007**, *39*, 2–9.

9   Y. X. Ren, S. L. Gao, S. P. Chen, B. J. Jiao, R. Z. Hu, Q. Z. Shi, *Chin. J. Chem*. **2004**, *22*, 1095−l101.

10   S. Yang, A. Navrotsky, *Chem. Mater.* **2002,** *14,* 2803-2811.

11   J. Chen, Y. Ma, G. Fan, Y. Li, J. Jiang, Z. Huang, *Mater. Lett*. **2011**, *65*, 1768−1771.

12   Z. Nan, M. Wang, B. Yan, *J. Chem. Eng. Data* **2009**, *54,* 83–89.

13   J. Wu, S. Chen, S. Gao, *Mater. Chem. Phys*. **2010**, *122*, 301–304.

14   Z. Lu, C. Gao, Q. Zhang, M. Chi, J. Y. Howe, Y. Yin, *Nano. Lett.* **2011**, *11*, 3404-3412.

15 (a) H. Deng, X.L. Li, Q. Peng, X. Wang, J.P. Chen, Y.D. Li, *Angew. Chem.* **2005**, *117*, 2842–2845; (b) P. Guo, L. Cui, Y. Wang, M. Lv, B. Wang, X.S. Zhao, *Langmuir* **2013**, *29*, 8997–9003.

16   Z. D. Lu, Y. D. Yin, *Chem. Soc. Rev.* **2012**, *41*, 6874–6887.

17   J. Liu, Y. Zhang, Z. Nan, *Mater. Res. Bull.* **2014**, *60*, 270–278.

18   S. E. Skrabalak, B. J. Wiley, M. Kim, E. V. Formo, Y. Xia, *Nano Lett.* **2008**, *8*, 2077-2081.

19   S. Krehula, S. Musić, Ž. Skoko, S. Popović, *J. Alloys Compd.* **2006**, *420*, 260-268.

20   L. S. Zhong, J. S. Hu, A. M. Cao, Q. Liu, W. G. Song, L. J. Wan, *Chem. Mater.* **2007**, *19,* 1648-1655.

21   L. S. Zhong, J. S. Hu, H. P. Liang, A. M. Cao, W. G. Song, L. J. Wan, *Adv. Mater.* **2006**, *18*, 2426–2431.

22   M. Niederberger, G. Garnweitner, *Chem. Eur. J.* **2006**, *12*, 7282 – 7302.

23   S. L. Jin, H. G. Deng, D. H. Long, X. J. Liu, L. Zhan, X. Y. Liang, W. M. Qiao, L. C. Ling, *J. Power Sources* **2011**, *196*, 3887-3893.

24   S. Gordon, C. Campbell, *Anal. Chem.* **1955**, *27*, 1102-1109.

25   Q. N. Zhang, Y. Zhang, C. Cai, Y. C. Guo, J. P. Reid, Y. H. Zhang, *J. Phys. Chem. A* **2014**, *118*, 2728-2737.

26   R. K. Selvan, V. Krishnan, C. O. Augustin, H. Bertagnolli, C. S. Kim, A. Gedanken, *Chem. Mater.* **2008**, *20*, 429-439.

27   B. S. Randhawa, *J. Mater. Chem.* **2000**, *10*, 2847-2852.

28   Y. Yang, L. L. Ren, C. Zhang, S. Huang, T. X. Liu, *ACS Appl. Mater. Interfaces* **2011**, *3*, 2779-2785.

29   L. S. Zhong, J. S. Hu, H. P. Liang, A. M. Cao, W. G. Song, L. J. Wan, *Adv. Mater.* **2006**, *18*, 2426-2431.

30   M. L. Wen, Q. Li, Y. Li, *J. Electron. Spectrosc. Relat. Phenom.* 2006, 153, 65-70.

31   P. Marcus, I. Olefjord, *Corros. Sci.* **1988**, *28*, 589-602.

32   S. Suzuki, T. Kosaka, M. Saito, H. Inoue, Y. Waseda, E. Matsubara, M. Oku, *Scripta. Mater.* **1997**, *36*, 841-845.

33   D. Brion, *Appl. Surf. Sci.* **1980**, *5*, 133-152.

34   W.P. Yang, D. Costa, P. Marcus, *J. Electrochem. Soc*. **1994**, *141*, 2669-2676.

35   T. L. Barr, *J. Phys. Chem.* 1978, 82, 1801-1810.

36   A. M. Beccaria, G. Poggi, G. Castello, *Br. Corros. J.* **1995**, *30*, 283-287.

37   P. Marcus, J.M. Grimal, *Corros. Sci.* **1992**, *33*, 805-814.

38   C.D. Wagner, W.M. Riggs, L.E. Davis, J.F. Moulder, Handbook of X-ray Photoelectron Spectroscopy, Perking-Elmer Corporation, Physical Electronics Division (1979)

39   L. Yang, Z. Wang, B. Zhai, Y. Shao, Z. Zhang, Y. Sun, J. Yang, *Ceram. Int.* **2013**, *39*, 8261-8266.

40   A. R. Brooks, C. R. Clayton, K. Doss, Y. C. Lu, *J. Electrochem. Soc.* **1986**, *133*, 2459-2464.

41   G. Fierro, G. M. Ingo, F. Mancia, *Corros.* **1989**, *45*, 814-823.

42   K. S. Kim, R. E. Davis, *J. Electron. Spectrosc. Relat. Phenom.* **1972**, *1*, 251-258.

43   A. B. Boese, Fink, C. K. In *Glycols*; Curme, G. O., Jr., Johnston, F., Eds.; Reinhold Publishing Corp.: New York, 1952; pp 125-126.

44   L. S. Zhong, J. S. Hu, H. P. Liang, A. M. Cao, W. G. Song, L. J. Wan, *Adv. Mater.* **2006**, *18*, 2426–2431

45   S. Kuai, Z. Nan, *J. Alloys Comp.* **2014**, *602*, 228–234.

46   G. R. Lee, J. A. Crayston, *Adv. Mater.* **1993**, *5*, 434.

47   R. C. Mehrotra, A. Singh, *Prog. Inorg. Chem.* **1997**, *46*, 239.

48   P. Druska, U. Steinike, V. Šepelák, *J. Solid State Chem.* **1999**, *146*, 13–21.

Table 1 Phases of the samples at different temperatures

sample	temperature (°C)	phase
A	90	L
B	99	G
C	103	G
D	107	G
E	118	G
F	134	L
G	159	S+L
H	187	S+L
I	200	S+L

*"L" means liquid phase, "G" means gel, and "S+L" means both of the liquid and

solid phases coexisted.

Table 2 Mass fractions of the metal ions and the molar ratios for the samples determined by ICP-OES and AAS.

Sample	mass fraction(%)	determined value	hypothesis value[*]	theoretical value[**]
B	Fe	14.82	15.60	16.61
	Na	9.406	10.62	10.26
	Zn	9.236	10.42	9.725
	Molar ratio(Fe:Na:Zn)	1.75 : 2.90 : 1	/	2 : 3 : 1
C	Fe	16.47	16.72	16.61
	Na	10.10	10.25	10.26
	Zn	9.462	9.60	9.725
	Molar ratio(Fe:Na:Zn)	2.04 : 3.04 : 1	/	2 : 3 : 1
D	Fe	16.59	16.63	16.61
	Na	10.21	10.24	10.26
	Zn	9.716	9.74	9.725
	Molar ratio(Fe:Na:Zn)	2.00 : 2.99 : 1	/	2 : 3 : 1
E	Fe	17.96	21.61	16.61
	Na	4.77	5.75	10.26
	Zn	9.646	11.60	9.725
	Molar ratio(Fe:Na:Zn)	2.18 : 1.41 : 1	/	2 : 3 : 1
G	Fe	23.7		
	Na	4.87		
	Zn	13.53		
	Molar ratio(Fe:Na:Zn)	2.05 : 0.36 : 1		
H	Fe	24.01		
	Na	4.43		
	Zn	11.07		
	Molar ratio(Fe:Na:Zn)	2.54 : 0.40 : 1		
I	Fe	27.29		
	Na	3.58		
	Zn	10.54		
	Molar ratio(Fe:Na:Zn)	3.03 : 0.34 : 1		

[*]: We hypothesized that $Fe_2(C_2H_4O_2)_3$, $ZnC_2H_4O_2$, and $NaNO_3$ were contained in the as-prepared samples, and the molar ratios of Fe, Zn, and Na were used as the determined values.

[**]: $Fe_2(C_2H_4O_2)_3$ and $ZnC_2H_4O_2$, and $NaNO_3$ were contained in the as-prepared samples, and the molar ratios of Fe, Zn, and Na were used as the initial ratios in the reaction systems..
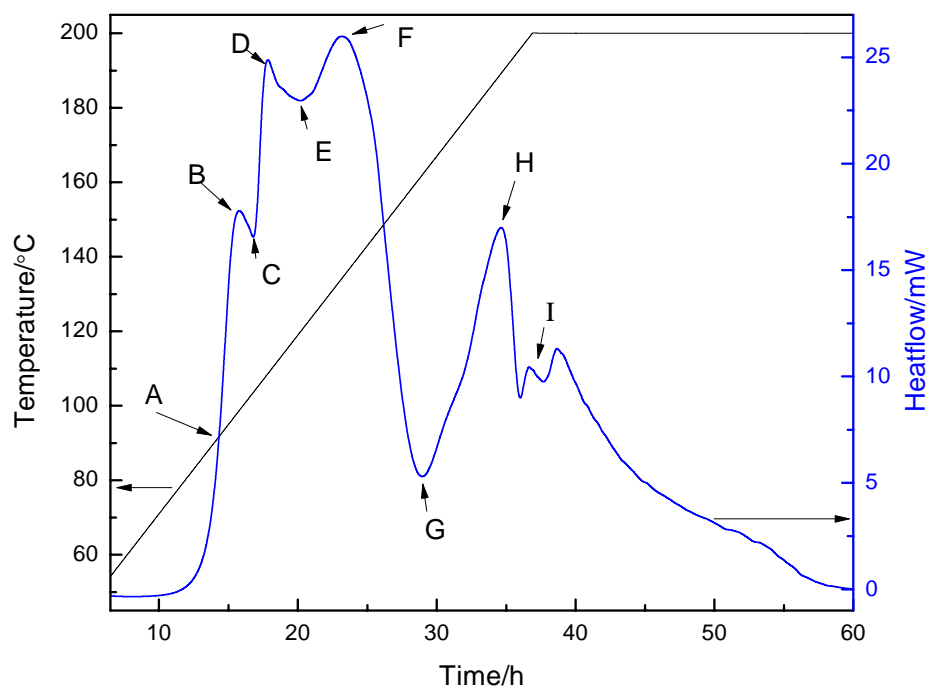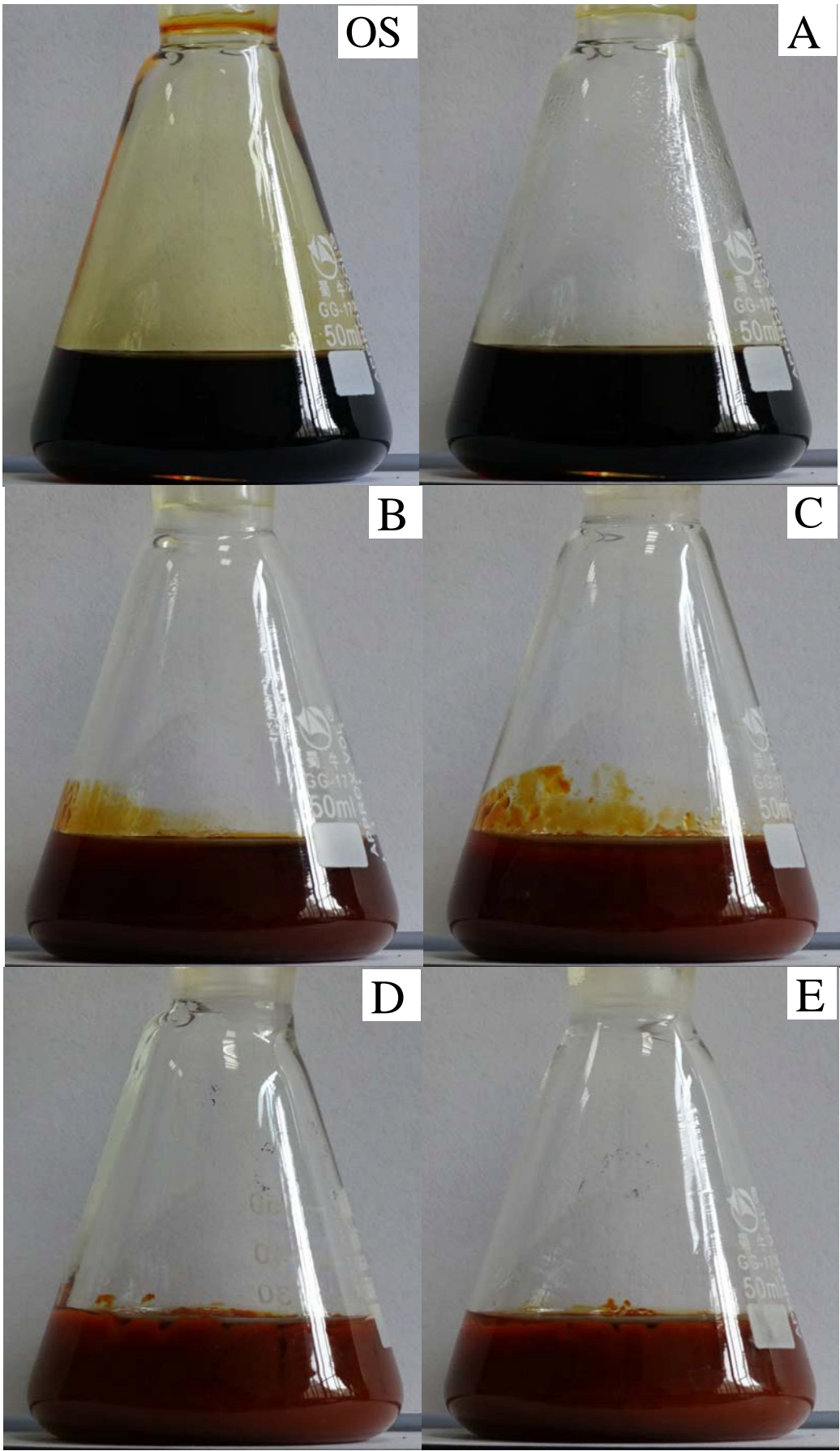
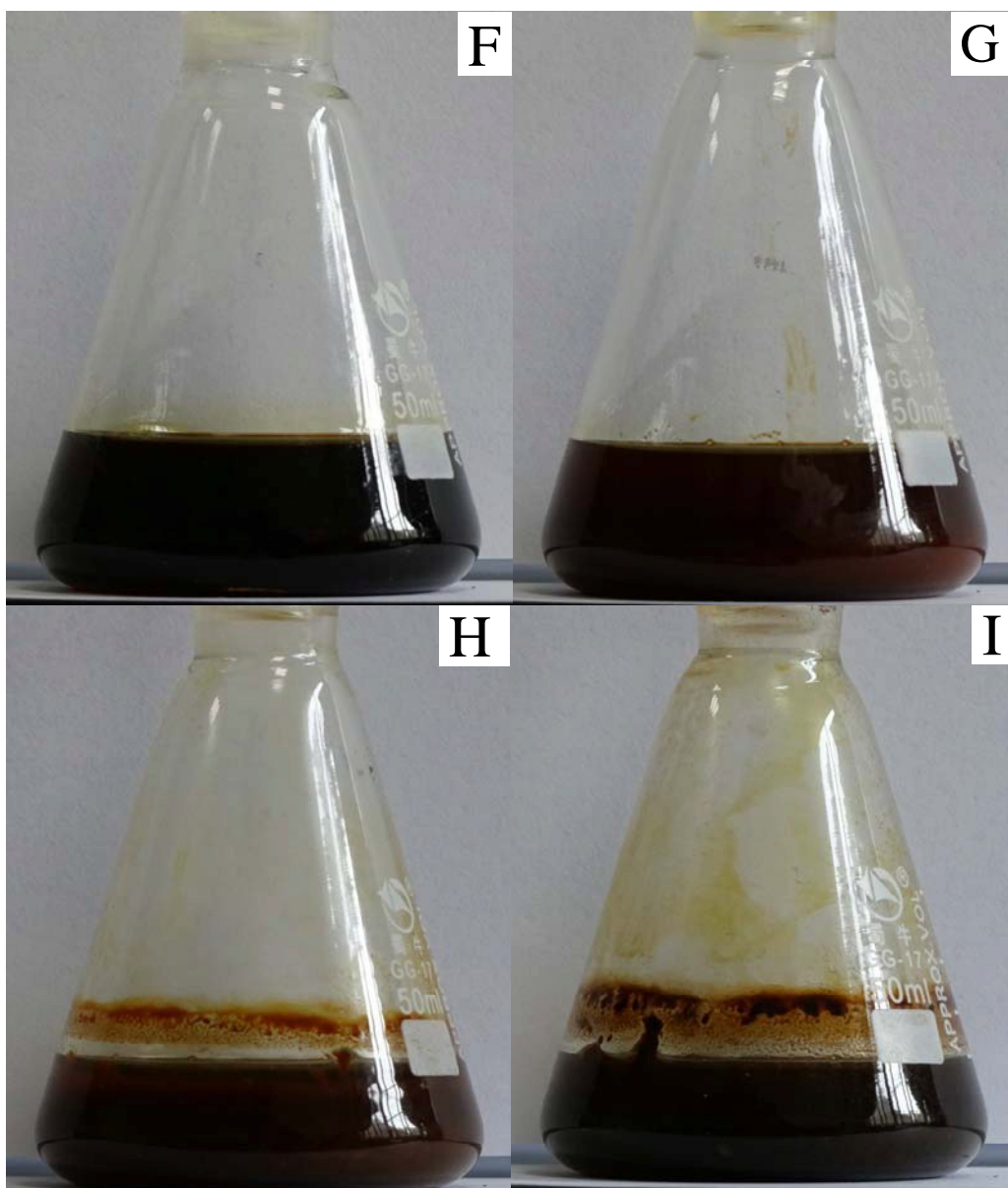**Figure 1**. Microcalorimetric curve for the $ZnFe_2O_4$ nanoparticles growth with the experimental temperature increase.

1

1

Figure 2. Photos of the reaction systems at different temperatures: OS, room temperature; A, 90 $^{\circ}$C; B, 99 $^{\circ}$C; C, 103 $^{\circ}$C; D, 107 $^{\circ}$C; E, 118 $^{\circ}$C; F, 134 $^{\circ}$C; G, 159 $^{\circ}$C; H, 187 $^{\circ}$C; I, 200 $^{\circ}$C.

2
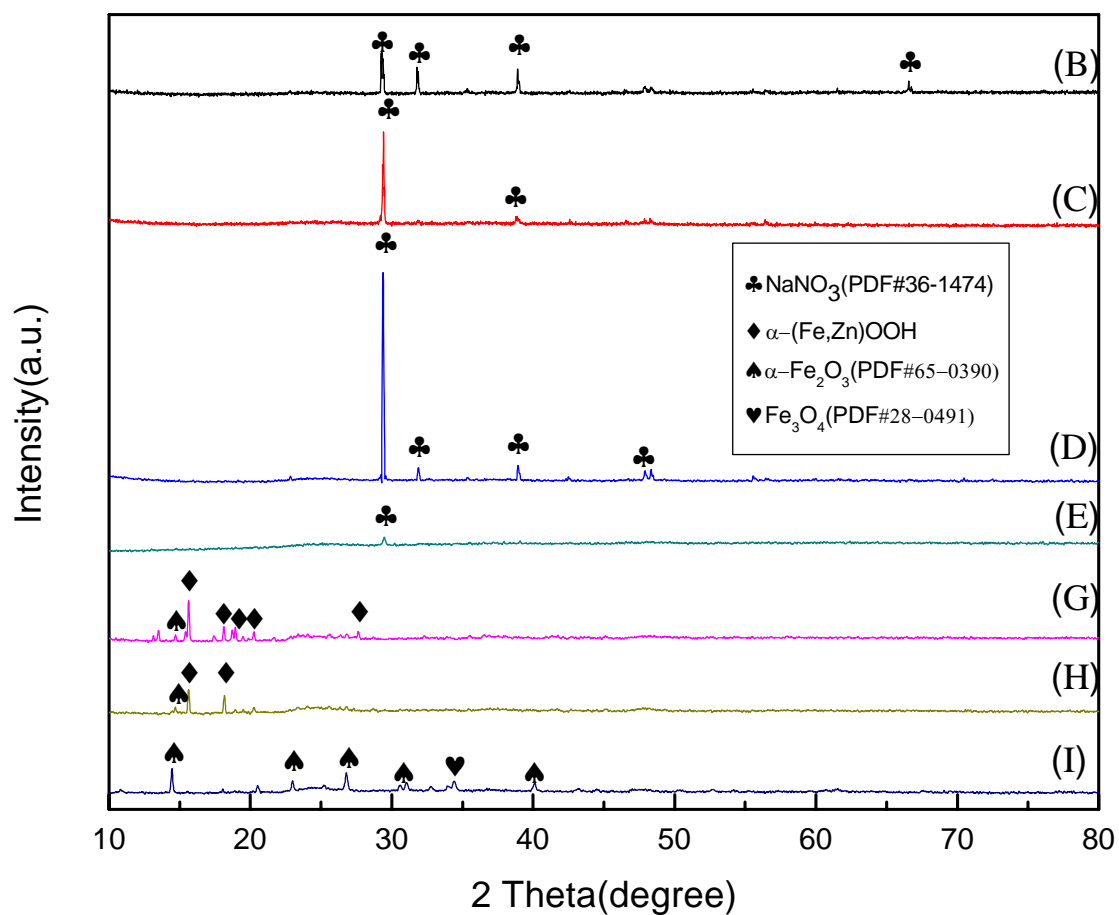
Figure 3. XRD diffraction patterns of the samples synthesized at different reaction temperatures, (B) 99 ^{o}C, (C) 103 ^{o}C, (D) 107 ^{o}C, (E) 118 ^{o}C, (G) 159 ^{o}C, (H) 187 ^{o}C, (I) 200 ^{o}C.

1
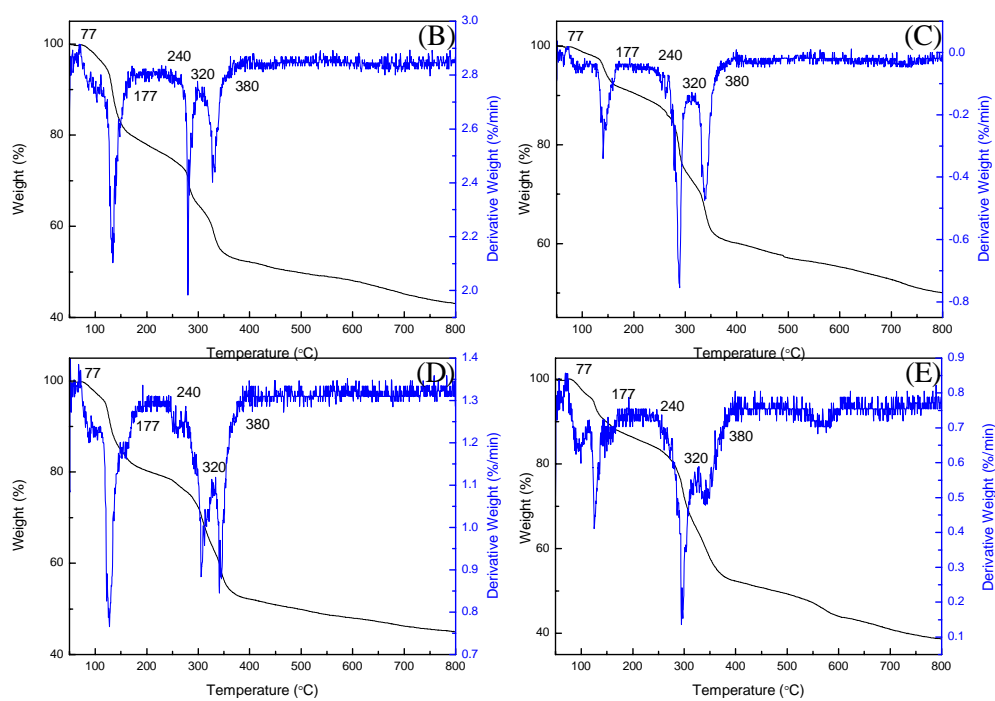
Figure 4. TG/DTG curves of the samples (*B*, *C*, *D*, and *E*) under argon.

1
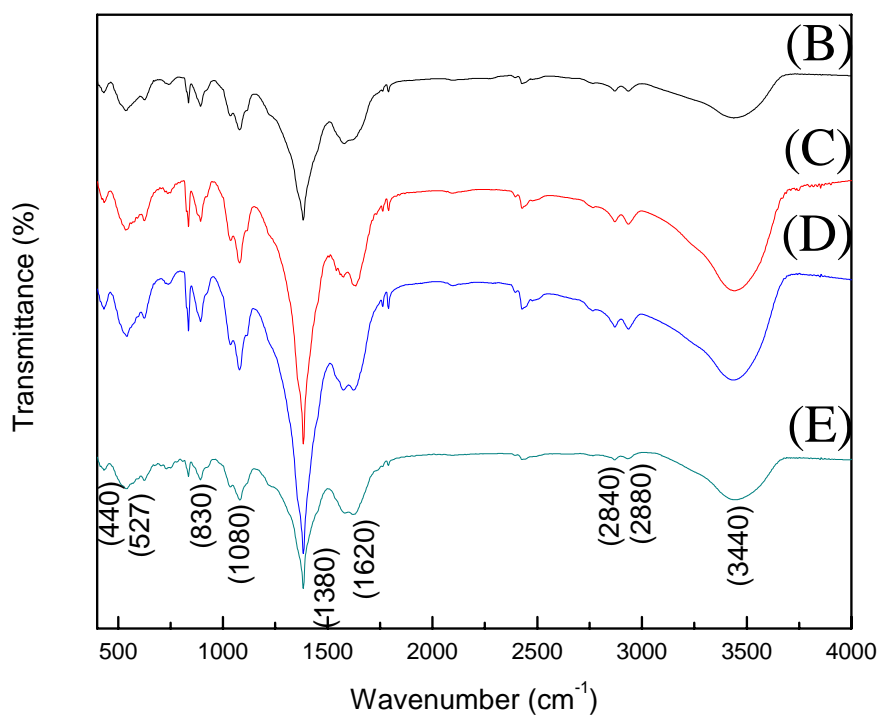
Figure 5. FTIR spectra of the samples synthesized at different reaction temperature,
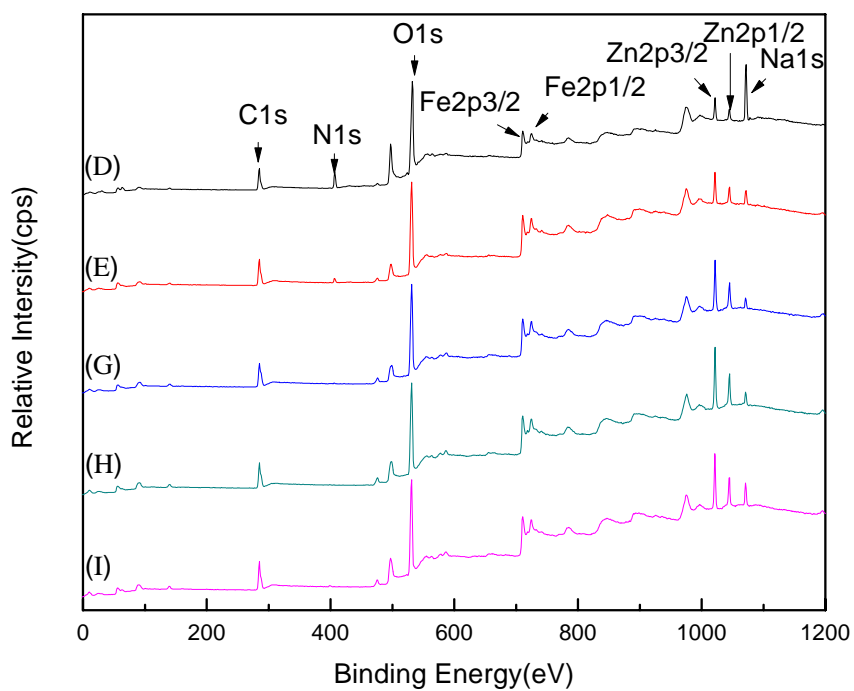
(B) 99 ^{o}C, (C) 103 ^{o}C, (D) 107 ^{o}C, (E) 118 ^{o}C.

1

Figure 6. XPS survey spectra of the samples synthesized at different reaction

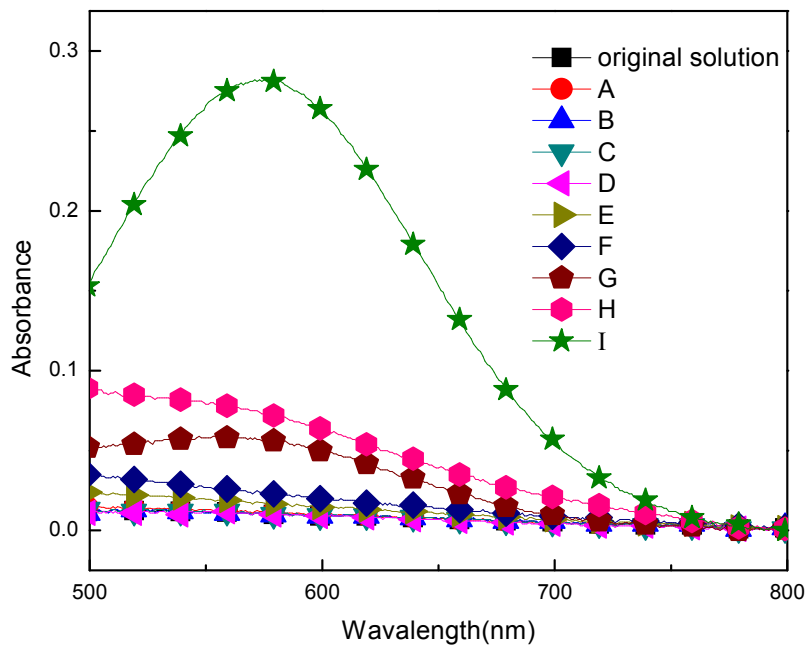temperatures, (D) 107 ^{o}C, (E) 118 ^{o}C, (G) 159 ^{o}C, (H) 187 ^{o}C, and (I) 200 ^{o}C.
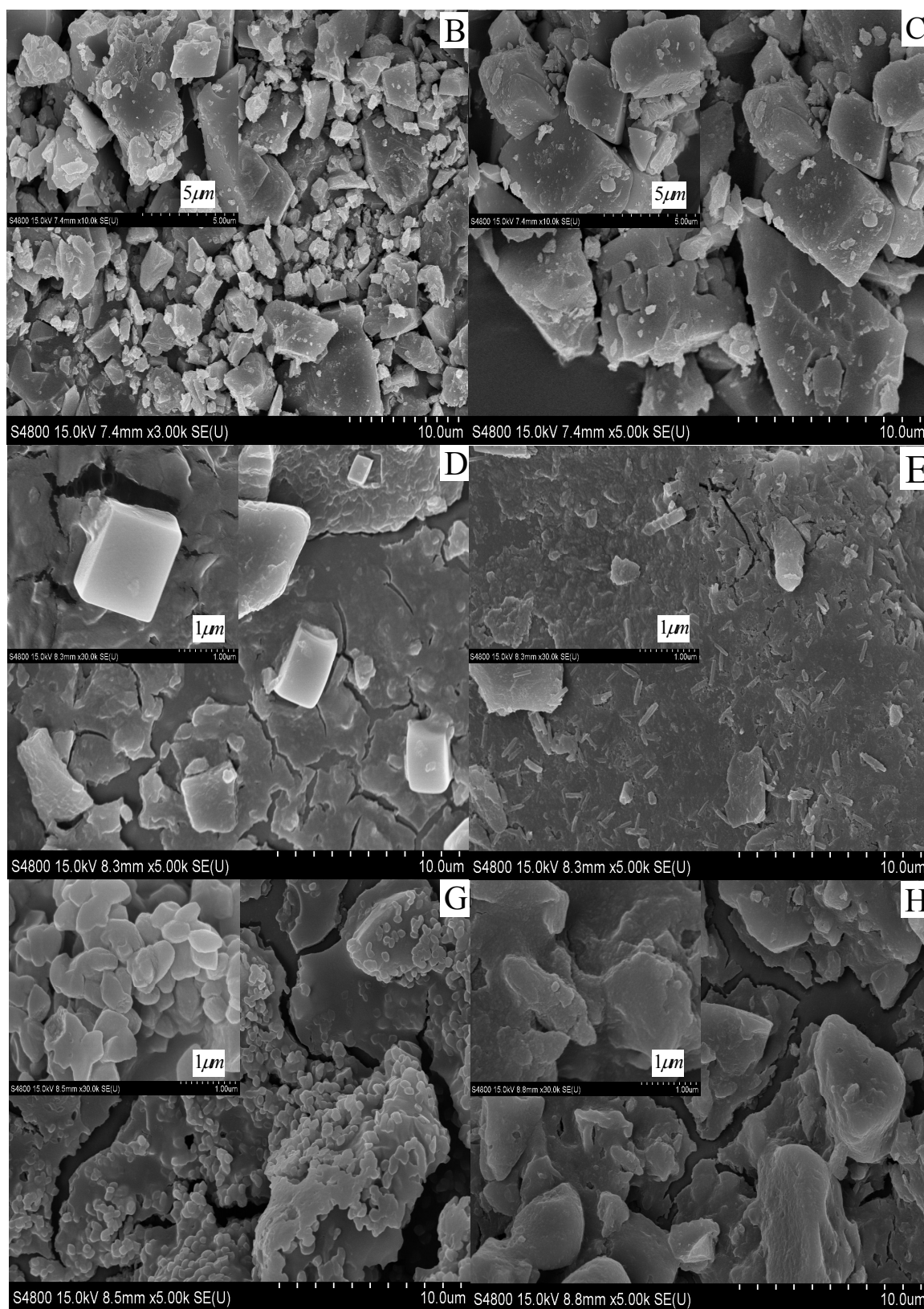
Figure 7. Absorbance spectra of the solutions at different reaction temperatures, (A)

90 ^{o}C, (B) 99 ^{o}C, (C) 103 ^{o}C, (D) 107 ^{o}C, (E) 118 ^{o}C, (F) 134 ^{o}C, (G) 159 ^{o}C,
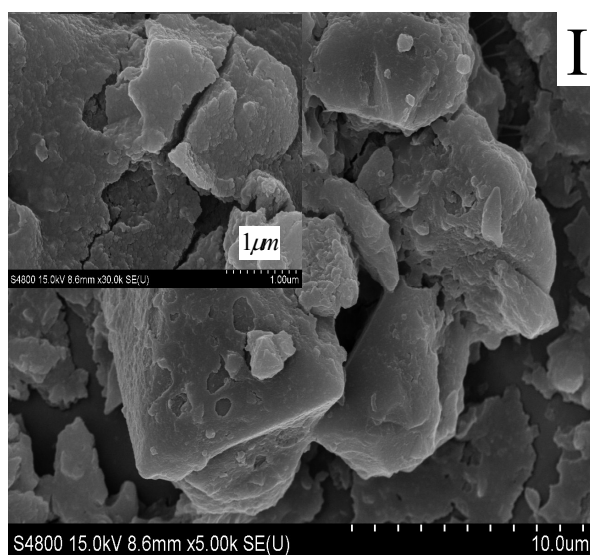
(H) 187 ^{o}C, and (I) 200 ^{o}C.

Figure 8. SEM images of the samples synthesized at different reaction temperatures, (B) 99 ^{o}C, (C) 103 ^{o}C,(D) 107 ^{o}C, (E) 118 ^{o}C, (G) 159 ^{o}C, (H) 187 ^{o}C, and (I) 200 ^{o}C. Insets show the magnified figures.